How to cite: *Angew. Chem. Int. Ed.* **2022,** *61,* e202208010
International Edition: doi.org/10.1002/anie.202208010
German Edition: doi.org/10.1002/ange.202208010

On-Surface Synthesis

Unusual Scaffold Rearrangement in Polyaromatic Hydrocarbons Driven by Concerted Action of Single Gold Atoms on a Gold Surface

Jesús I. Mendieta-Moreno, Benjamin Mallada, Bruno de la Torre, Timothée Cadart, Martin Kotora, and Pavel Jelínek**

Abstract: Chemical transformation of polyaromatic hydrocarbon (PAH) molecules following different reaction strategies has always been the focus of organic synthesis. In this work, we report the synthesis of a PAH molecule, formation of which consists of an unusual C–C bond cleavage accompanied by a complex π-conjugated molecular scaffold rearrangement. We demonstrate that the complex chemical transformation is steered by concerted motion of individual Au^0 gold atoms on a supporting Au(111) surface. This observation underpins the importance of single-atom catalysis mediated by adatoms in on-surface synthesis as well as catalytic activity of single Au^0 atoms facilitating cleavage of covalent carbon bonds.

Introduction

Emergence of on-surface synthesis of organic molecules on metal surfaces under ultra-high vacuum (UHV) conditions within the last two decades enabled chemical transformations that would be difficult to achieve using traditional solution-based chemistry. Precursors are structurally divergent aromatic compounds that are either transformed into products possessing a reorganized skeletal framework or to larger polyaromatic hydrocarbon (PAH) molecules such as nanographenes or π-conjugated polymers.[1–7]

[*] Dr. J. I. Mendieta-Moreno, B. Mallada, Dr. B. de la Torre, Prof. Dr. P. Jelínek
Institute of Physics of Czech Academy of Sciences
16200 Prague (Czech Republic)
E-mail: jelinekp@fzu.cz

B. Mallada, Dr. B. de la Torre, Prof. Dr. P. Jelínek
Regional Centre of Advanced Technologies and Materials,
Czech Advanced Technology and Research Institute (CATRIN),
Palacký University Olomouc
78371 Olomouc (Czech Republic)

B. Mallada
Department of Physical Chemistry,
Palacký University Olomouc
Str. 17. listopadu 12, 771 46 Olomouc (Czech Republic)

Dr. T. Cadart, Prof. Dr. M. Kotora
Department of Organic Chemistry, Charles University
128 00 Prague 2, (Czech Republic)
E-mail: kotora@natur.cuni.cz

The choice of surface can significantly affect the nature of the interaction **Precursor** and the surface from physisorption to chemisorption,[8–10] and thus, the course of chemical transformations.[1,2] At the higher temperatures, which are necessary for the initiation of most on-surface reactions, the presence of individual atoms diffusing on the surface from the atomic steps also cannot be ruled out. It can be assumed that these adatoms play an important role in the initiation of the chemical reaction itself; for example, in the cycloaddition[11] or Ullmann coupling.[12–15] However, a detailed understanding of their significance and role in these chemical transformations on metal surfaces is still not complete. For example, one of the unanswered questions remains whether one or more adatoms, including their concerted action, are needed for selected chemical transformations.

Herein, we aim to elaborate more on our understanding of the role of gold adatoms in on-surface synthesis. It is well-known that Au(111) shows a relatively low chemical reactivity compared to other surfaces of transition metals.[16] At the same time, low-coordination gold atoms present on the atomic surface steps,[17] in one-dimensional chains[18] or nanoclusters,[19] show enhanced chemical reactivity.

Although small clusters of gold atoms can catalyze various chemical transformations,[20–22] the role of single gold-adatoms in C–C bond activation and cleavage reactions is essentially unexplored. In fact, only Au^I-catalyzed ring opening of the strained biphenylenes has been reported so far.[23–26] Presumably, the whole process should be facilitated by participation of several single gold atoms on the Au(111) surface. This is supported by recent observations that the gold-catalyzed processes in solutions require concomitant participation of several gold atoms; for example, dinuclear gold catalysis.[27]

Above room temperature, surface diffusion of individual gold atoms detached from atomic steps on surfaces, so-called adatoms, takes place. These low coordination adatoms show negligible charge transfer with the Au(111) surface, so they have a zero oxidation state Au^0. Existence and the crucial effect of Au adatoms has been clearly demonstrated; for example, in depiction of sulfur or thiolate on a gold surface.[22,28–30] Hence, it is reasonable to assume that the Au adatoms, as highly unsaturated and mobile single Au^0 atoms, may play a significant role in the C–C and C–H bond cleavage steps.

In this work, we will focus on on-surface chemical transformation of non-planar PAH molecules. This transformation is driven by internal stress imposed on the

molecular skeleton due to dispersion forces acting between the precursor and the surfaces. As typical examples of such transformation from a 3D to 2D molecular framework can serve the conversion of a [7]helicene to a planar corannulene derivative (on an Ag(111) surface),[31] or the transformation of helical compounds with the azulene moieties to planar species with the fulvalene segments (on a Cu(001) surface).[32] The deposition of helical compounds on metal surfaces have been reported, albeit their further transformations have not been studied.[33–35] Also, polyaromatic compounds, considered as flat cmopounds, can be converted to compounds possessing non-hexagonal four, five, and seven-membered rings as well. They include substances such as curved nanographenes with regularly fused heptagons and pentagons,[36] helical nanographenes with azulene units,[37] non-benzenoid nanographenes,[38] polyazulene nanoribbons,[39] or non-Kekulé aromatic hydrocarbons.[40] Other processes that occur during skeletal rearrangements are C–C bond cleavage reactions resulting in the loss of carbon fragments. Demethylation during the thermally induced on-surface cyclization of 4,10-bis(2′-bromo-4-methylphenyl)-1,3-dimethylpyrene to form the nonalternant PAH diindeno[1,2,3-*cd*:1′,2′,3′-*mn*] pyrene on Au(111) serve as a typical example.[41]

Recently, we have studied thermally activated planarization of precursor on an Au surface at different temperatures, leading to synthesis of non-benzenoid non-alternant PAH products (for further details see ref. [42]). We found that the major planar products formed in the range of 525–575 K were either **P1** or **Moth** (Figure 1), along with other substances, depending on the annealing temperature.[42] In that work, we employed a combination of scanning tunneling / noncontact atomic force microscopy (STM/nc-AFM) high-resolution experiments with quantum and molecular mechanical (QM/MM) simulations to understand the reaction pathways from **Precursor** leading to the formation of **P1** and other formed substances. Namely, we rationalized the reaction course towards **P1** product in terms of cyclodehydrogenation and cycloaddition reactions, 1,2-aryl shifts, and demethylation.[42]

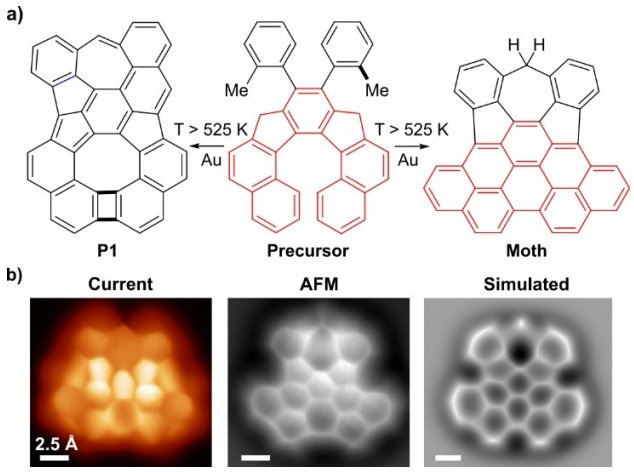

Figure 1. Rearrangement of **Precursor** to **P1** or **Moth** on the Au(111) surface upon thermal annealing. a) The reaction course driven by thermal annealing at $T > 525$ K from the **Precursor** to two most frequent products **P1** and **Moth**, see ref. [27]. b) High-resolution STM (left) and nc-AFM (center) images acquired with a CO-tip of Moth on Au(111) using constant height mode at bias voltage $V = 5$ meV. Simulated AFM image of **Moth** with a CO-tip (right).

On the other hand, the reaction pathway yielding compound **Moth** possessing the phenanthro(2.1,10,9,8,7-*pqrstuv*)pentaphene framework proved to be a rather challenging task, which remains to be elucidated. Although aromatization and planarization of the molecule are the overall driving forces of the skeletal reorganization, the course of individual steps is difficult to fathom based on known reaction mechanisms in solution, at the first glance. Therefore, there is a quest for detailed understanding of the reaction mechanism leading to **Moth**, which is the subject of this work.

As a starting point, the overall rearrangement of the **Precursor's** basic core to **Moth** cannot be explained by a sequence of 1,2-aryl shifts (Stone–Wales rearrangement).[43,44] The respective scaffolds involved in the rearrangement are highlighted in red in Figure 1. Transformation of the benzo[*c*]benzo[6,7]indeno[2,1-*c*]fluorene scaffold in **Precursor** to phenanthro(2.1,10,9,8,7-*pqrstuv*)-pentaphene in **Moth** would formally require an unusual 1,3-aryl shift.[45]

Another mechanism could be rearrangement by radical-induced processes similar to those proposed by Kartney et al. for the rearrangement of triphenylenes.[46] Following this line of thought, the first step would involve the cleavage of an Csp^2–Csp^3 bond of the dibenzocyclopentadiene ring resulting in the formation of a biradical. This biradical would undergo a series of complex chemical rearrangements including 1,5-hydrogen shifts along with rotation(s) of molecular fragments. However, the initial cleavage of the Csp^2–Csp^3 bond in the dibenzocyclopentadiene moiety would require elevated activation energy not accessible under the experimental conditions. For example, the bond dissociation energy (BDE) analysis for biphenylene[47] is 57 kcal mol^{-1} whereas the one for fluorene would be 90 kcal mol^{-1},[48] and for indene it was calculated to be 61 kcal mol^{-1} at 1300 K.[49] In view of the above arguments, it is evident that none of the discussed scenarios can easily explain the reaction mechanism of the **Moth** with relatively high yield compared to other products.

Results and Discussion

In view of the aforementioned, we looked for an alternative and more feasible rationale of the reaction course in the presence of single Au adatoms. In addition, the following question arises: does the rearrangement take place independently at each molecular side or are both rearranged concomitantly?

We carried out quantum mechanical calculations to shed light on a probable course of the chemical transformation stimulated by Au^0 adatoms, as depicted in Scheme 1a. Here, we employed quantum and molecular mechanical (QM/MM)[50] simulations to ensure computational feasibility of

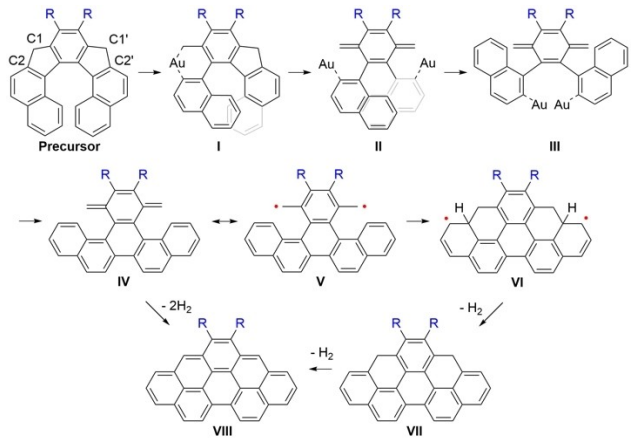

Scheme 1. View of the transformation of **Precursor** (R = *o*-tolyl) to VIII.

the free energy calculations of the activation barriers for selected reaction steps, including C–C bond breakage/formation in the reaction Scheme 1. In such QM/MM calculations, the molecule and Au adatoms were involved in the QM region, while the underlying surface was treated in the MM region. Previous studies[15,51] have shown that this QM/MM approach provides a reasonably accurate description of the chemical reactions involving adatoms.

In the first step of the transformation, as shown in Movie S1, a single Au adatom interacts via dispersive force with the most elevated dibenzocyclopentadiene moiety, which places it in between the surface and the molecule (Figure 2d). According to our calculations, this stable initial configuration enables the cleavage of the adjacent C1–C2 bond. Figure 2a shows a calculated free energy activation barrier of 20 kcal mol^{-1} along a reaction coordinate, defined as the C1–C2 bond length. This process with a relatively low activation barrier leads to the **intermediate** state **I** where the Au adatom is covalently bonded to both C1 and C2 carbon atoms, as shown in Figure 2e. Figure 2c displays an evolution of the bond lengths between the Au adatom and two C1 and C2 carbon atoms, respectively, along the reaction coordinate. Interestingly, a dihedral angle Φ between C1 and C2 carbons remains constant along the reaction coordinate (for definition of Φ see Figure S1). The constant value of the dihedral angle Φ indicates, that the formation of the covalent bonds between C1 and C2 carbon atoms and the Au adatom, in the **intermediate** state **I**, preserves original hybridization character of carbon atoms sp^3 (C1) and sp^2 (C2), respectively. This configuration avoids formation of radical state in **intermediate I**.

Following the Scheme 1, the second step consists of a similar process involving the cleavage of the C1′–C2′ bond of the second dibenzocyclopentadiene moiety (Figure 2b). This step takes place in a similar way, including the second Au adatom interacting at the opposite side of the molecule (Figure 3d; see also Movie S1). Similarly, the Au adatom acts as a catalyst for the cleavage of the C1′–C2′ bond through a free energy barrier of 22 kcal mol^{-1} (Figure 3a). The transition state corresponds to the structure where both carbon atoms are covalently bonded to the second Au adatom. However, in the **intermediate II**, each Au adatom remains bonded only to C2 or C2′ carbon atoms of the naphthalene moiety II (Figure 3c and e). We can observe that the bond formed in step 1 between C1 and Au adatom on the opposite side of the molecule breaks at the end of this reaction course (Figure 3c). This allows both carbon atoms, C1 and C1′, to adopt sp^2 hybridization, which can be evaluated from the evolution of dihedral angle Φ (Figure 3b)

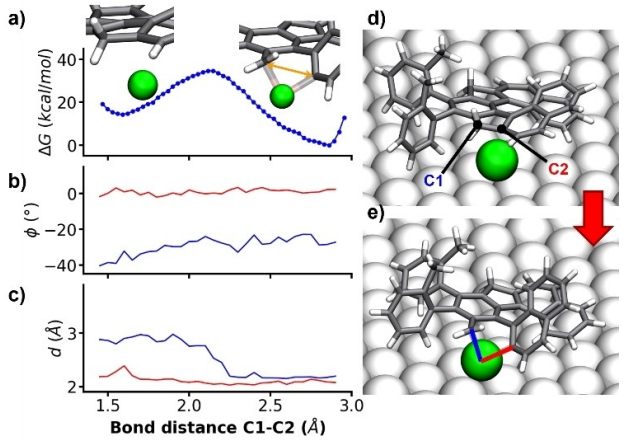

Figure 2. Step 1 of the reaction. a) Free energy calculation of step 1. Insert with a magnification of the initial and final states with the reaction coordinate in orange. b) Dihedral angle evolution during step 1 of the reaction for C1 (blue) and C2 (red); for definition of the dihedral angle see Figure S1. c) Distance evolution during step 1 reaction for C1-Adatom1 (blue) C2-Adatom1 (red). d) Geometry of the initial state. e) Geometry of the final state with the distances C1-Adatom1 (blue) C2-Adatom1 (red). See also Movie S1.

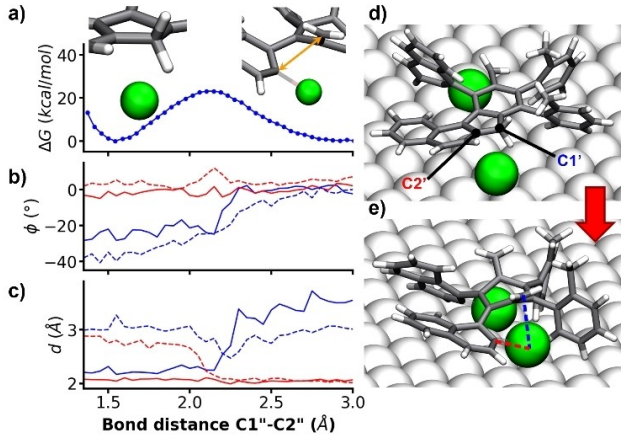

Figure 3. Step 2 of the reaction. a) Free energy calculation of step 2. Insert with a magnification of the initial and final states with the reaction coordinate in orange. b) Dihedral angle evolution during step 2 of the reaction for C1 (blue), C1′ (dashed blue), C2 (red), and C2′ (dashed red). c) Distance evolution during step 2 reaction for C1-Adatom1 (blue) C2-Adatom1 (red), C1′-Adatom2 (dashed blue) C2′-Adatom2 (dashed red). d) Geometry of the initial state. e) Geometry of the final state with the distances C1′-Adatom1 (dashed blue) C2′-Adatom1 (dashed red). See also Movie S1.

with the final value near 0°, which is characteristic for sp^2 hybridization. These changes in distances and angles are related also to the orbital rearrangement of the central benzene ring that becomes non-aromatic at the end of the step 2. These orbital rearrangements are possible due to the concerted action of both adatoms with the molecule (Movie S1). In addition, the interaction between the Au adatom and the naphthalene moieties increases at the end of this step. Such circumstances favor the molecular complex adopting a new configuration, **intermediate III**, where two Au atoms form a dimer (Figure 4c). The process is accompanied by a simultaneous rotation of two naphthalene moieties. Importantly, the concerted action of Au adatoms, accompanied by the rotation, play a pivotal role in the shift reaction towards the final **Moth** product. The presence of the Au dimer facilitates a subsequent formation of covalent bond between two naphthalene moieties later on. Importantly, **intermediate III** has a lower energy ($\Delta = -24$ kcal mol^{-1}) than the one shown in Figure 3d.

In the next reaction step, a new covalent C2–C2′ bond is formed from the merger of two naphthalene units. In this reaction step, the presence of the Au dimer directs the formation of a covalent bond between C2 and C2′ carbon atoms where each one is bound to one Au atom of the dimer. In this final state (Figure 4b and d), the Au dimer is not covalently bonded to the molecular scaffold and it may diffuse on the surface, as shown in Movie S1. Importantly, our QM/MM calculations show this process has a low free energy barrier of 15 kcal mol^{-1} (Figure 4a). Resulting **intermediate IV** possesses the picene molecular scaffold characteristic of the **Moth** molecule.

To underline the key role of Au adatoms in the above-described chemical transformation, we calculated the free energy of the activation barrier as well without the presence of the Au adatoms for step 1 and step 2. We observed, not only significantly higher activation energies (≈ 100 kcal mol^{-1}), but also formation of the final products is less energetically favorable (Figures S2 and S3). These findings clearly indicate that the proposed chemical transformation is not feasible without direct involvement of individual Au adatoms.

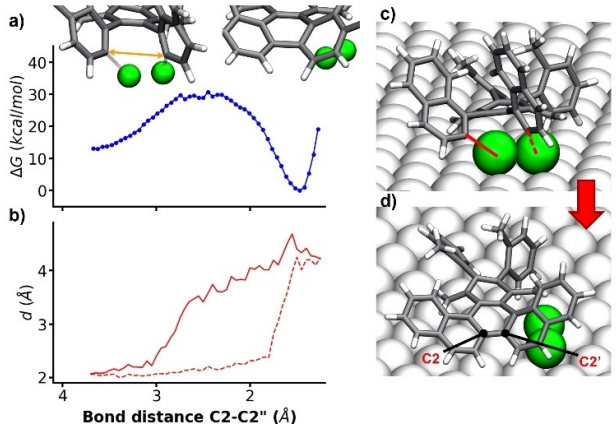

Figure 4. Step 3 of the reaction. a) Free energy calculation of step 3. Insert with a magnification of the initial and final states with the reaction coordinate in orange. b) Distance evolution during step 3 of the reaction for C2-Adatom1 (red) C2′-Adatom2 (dashed red). c) Geometry of the initial state with the distances C2-Adatom1 (red) C2′-Adatom1 (dashed red). d) Geometry of the final state. See also Movie S1.

In the subsequent text, we will tentatively discuss the course of the remaining chemical transformation towards **Moth** product. The highly reactive *p*-quinodimethane (PQDM) moiety is present in intermediate **IV**. PQDM has been shown to be favorable for undergoing cyclodimerization towards para[2,2]cyclophane[52] or cyclotrimerization to [2.2.2]paracyclophane.[53] Similar radical reactions have also been observed for other diradicals, such as 6,12-diethynylindeno[1,2-*b*]fluorenes.[54] In this respect, calculations showed that triplet PQDM has significantly lower barriers to react with unsaturated substances (e.g., ethylene) in comparison to other radical species.[55] Thus, we calculated the biradical index of **VI** to be y0 = 0.265, which seems to be low but not negligible to discard completely the radical cyclization mechanism.

Hence, we assumed that given the partial planar character of **V**, the diradical would attack neighboring aromatic rings forming diradical **VI**. Several pathways could be envisioned from this point. It should be emphasized that the driving force of all subsequent reaction pathways are directed to increase the aromaticity of the system. First, the simplest pathway from **VI** would proceed through abstraction of H_2 forming **VII**. Then the compound succumbs to additional dehydrogenation induced by the gold adatom/surface to compound **VIII**, giving rise to the final pentaphene structure of the **Moth** molecule. Second, one of the radicals in **VI** could migrate via a series of 1,3-rearrangements to form compound **VII** (Scheme S1). Finally, compound **VII** could then undergo two dehydrogenations to give **VIII**.

Alternatively, we cannot exclude a scenario that includes cyclodehydrogenation of **IV** directly to **VIII** via interaction with Au adatoms. This process is initiated by dehydrogenation on the methane group by the Au adatom. This process can be further supported by internal stress imposed by dispersion forces on the non-planar molecule on the surface.

The last steps of the formation of the **Moth** product involves demethylation and cyclodehydrogenation of *o*-tolyl groups (in blue in Scheme 2). The transformation is driven by mechanical strain imposed on the non-planar phenyl unit due to the dispersion interaction between the product **VIII** and the Au surface, as already discussed in the previous work.[42] The course of the reaction is strongly influenced by orientation of the *o*-tolyl groups with respect to the underlying surface. Namely, the *o*-tolyl groups are preferentially oriented outwards from the surface (Figure S4). Indeed, this arrangement maximizes the dispersion forces acting between the molecular skeleton and the Au(111) substrate. Scheme 2 depicts a tentative reaction course towards the **Moth** product. According to the QM/MM simulations, the product **VIII** preferentially adopts a configuration consisting of inclined *o*-tolyl groups with the methyl group pointing out of the surface (see Figure S5). This configuration facilitates a cleavage of the methyl group of one of the *o*-tolyl groups

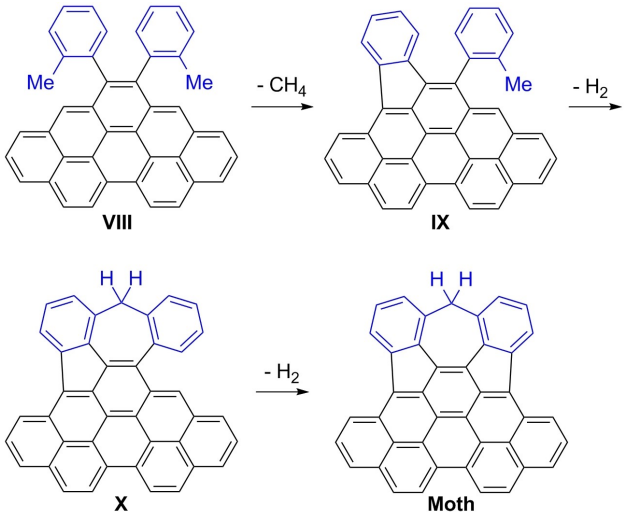

Scheme 2. The final steps from **VII** towards the formation of **Moth**.

inducing a formation of product **IX** with the new five-membered ring. In next step, according to QM/MM simulations, the methyl group of the *o*-tolyl functionality prefers to be oriented towards the planarized phenyl (Figure S6), which fosters the formation of the seven-membered ring (compound **X**), accompanied by release of a H_2 molecule. Finally, the planar **Moth** molecule is formed by a dehydrogenation process and subsequent formation of a five-membered ring.

Conclusion

In summary, we reported the unusual rearrangement of a π-conjugated scaffold steered by concerted action of two Au^0 adatoms on the Au(111) surface. This complex arrangement, which has not yet been described in solution chemistry, shows the potential of the on-surface chemistry to examine new hitherto unexplored reaction mechanisms, including single metal atoms as catalysts. The atypical C–C bond cleavage facilitated by Au^0 adatoms not only demonstrates their catalytic capability but also general importance of adatoms in on-surface reactions. We believe that the catalytic activity of Au^0 adatoms on supporting surfaces can be extended to other C–C bond cleavage or uncharted chemical shifts. Our results highlight the possibility of a concerted action of adatoms on surfaces as well. This factor may enrich current strategies for formation of novel compounds not available by traditional catalytic routes. In summary, we believe that this work can stimulate more elaborate studies exploiting the concept of single-atom catalysis driven by metal adatoms on supporting surfaces as well as their coordinated action.

Acknowledgements

This work was supported by the Czech Science Foundation grant No. 21-39639L (M.K.) and 20-13692X (J.M. P.J., B.M.). This work has been supported by Praemium Academie of the Academy of Science of the Czech Republic. B.T. acknowledges support from the Ministry of Education, Youth and Sports of the Czech Republic CZ.02.1.01/0.0/0.0/16_019/0000754. B.M. acknowledges support from the Internal Student Grant Agency of the Palacký University in Olomouc, Czech Republic, IGA_PrF_2022_026 and a Fischer scholarship. Computational resources were provided by the CESNET LM2015042 and the CERIT Scientific Cloud LM2015085, provided under the program "Projects of Large Research, Development, and Innovations Infrastructures".

Conflict of Interest

The authors declare no conflict of interest.

Data Availability Statement

The data that support the findings of this study are available from the corresponding author upon reasonable request.

Keywords: (PAH) Polyaromatic Hydrocarbon · (SPM) Scanning Probe Microscopy · on-Surface Synthesis

[1] S. Clair, D. G. de Oteyza, *Chem. Rev.* **2019**, *119*, 4717–4776.
[2] T. Wang, J. Zhu, *Surf. Sci. Rep.* **2019**, *74*, 97–140.
[3] L. Dong, P. N. Liu, N. Lin, *Acc. Chem. Res.* **2015**, *48*, 2765–2774.
[4] F. Klappenberger, Y.-Q. Zhang, J. Björk, S. Klyatskaya, M. Ruben, J. V. Barth, *Acc. Chem. Res.* **2015**, *48*, 2140–2150.
[5] Q. Fan, J. M. Gottfried, J. Zhu, *Acc. Chem. Res.* **2015**, *48*, 2484–2494.
[6] B. Yang, B. Dong, L. Chi, *ACS Nano* **2020**, *14*, 6376–6382.
[7] A. Sánchez-Grande, B. de la Torre, J. Santos, B. Cirera, K. Lauwaet, T. Chutora, S. Edalatmanesh, P. Mutombo, J. Rosen, R. Zbořil, R. Miranda, J. Björk, P. Jelínek, N. Martín, D. Écija, *Angew. Chem. Int. Ed.* **2019**, *58*, 6559–6563; *Angew. Chem.* **2019**, *131*, 6631–6635.
[8] S. J. Jenkins, *Proc. R. Soc. A* **2009**, *465*, 2949–2976.
[9] W. Liu, A. Tkatchenko, M. Scheffler, *Acc. Chem. Res.* **2014**, *47*, 3369–3377.
[10] S. Simpson, E. Zurek, *J. Phys. Chem. C* **2012**, *116*, 12636–12643.
[11] O. Díaz Arado, H. Mönig, H. Wagner, J.-H. Franke, G. Langewisch, P. A. Held, A. Studer, H. Fuchs, *ACS Nano* **2013**, *7*, 8509–8515.
[12] Z. Zhang, D. F. Perepichka, R. Z. Khaliullin, *J. Phys. Chem. Lett.* **2021**, *12*, 11061–11069.
[13] C. J. Judd, F. L. Q. Junqueira, S. L. Haddow, N. R. Champness, D. A. Duncan, R. G. Jones, A. Saywell, *Commun. Chem.* **2020**, *3*, 166.
[14] M.-T. Nguyen, C. A. Pignedoli, D. Passerone, *Phys. Chem. Chem. Phys.* **2011**, *13*, 154–160.

[15] M. Telychko, J. Su, A. Gallardo, Y. Gu, J. I. Mendieta-Moreno, D. Qi, A. Tadich, S. Song, P. Lyu, Z. Qiu, H. Fang, M. J. Koh, J. Wu, P. Jelínek, J. Lu, *Angew. Chem. Int. Ed.* **2019**, *58*, 18591–18597; *Angew. Chem.* **2019**, *131*, 18764–18770.
[16] B. Hammer, J. K. Norskov, *Nature* **1995**, *376*, 238–240.
[17] M. Mavrikakis, P. Stoltze, J. K. Nørskov, *Catal. Lett.* **2000**, *64*, 101–106.
[18] P. Jelínek, R. Pérez, J. Ortega, F. Flores, *Phys. Rev. Lett.* **2006**, *96*, 046803.
[19] L. Liu, A. Corma, *Chem. Rev.* **2018**, *118*, 4981–5079.
[20] A. S. K. Hashmi, *Chem. Rev.* **2007**, *107*, 3180–3211.
[21] S. A. Shahzad, M. A. Sajid, Z. A. Khan, D. Canseco-Gonzalez, *Synth. Commun.* **2017**, *47*, 735–755.
[22] P. Carro, R. C. Salvarezza, *Nanoscale* **2019**, *11*, 19341–19351.
[23] M. Joost, L. Estévez, K. Miqueu, A. Amgoune, D. Bourissou, *Angew. Chem. Int. Ed.* **2015**, *54*, 5236–5240; *Angew. Chem.* **2015**, *127*, 5325–5329.
[24] C.-Y. Wu, T. Horibe, C. B. Jacobsen, F. D. Toste, *Nature* **2015**, *517*, 449–454.
[25] A. Zeineddine, L. Estévez, S. Mallet-Ladeira, K. Miqueu, A. Amgoune, D. Bourissou, *Nat. Commun.* **2017**, *8*, 565.
[26] H. Takano, S. Okazaki, S. Nishibe, T. Ito, N. Shiozawa, N. Sugimura, K. S. Kanyiva, T. Shibata, *Org. Biomol. Chem.* **2020**, *18*, 5826–5831.
[27] W. Wang, C.-L. Ji, K. Liu, C.-G. Zhao, W. Li, J. Xie, *Chem. Soc. Rev.* **2021**, *50*, 1874–1912.
[28] Z. Feng, S. Velari, A. Cossaro, C. Castellarin-Cudia, A. Verdini, E. Vesselli, C. Dri, M. Peressi, A. de Vita, G. Comelli, *ACS Nano* **2015**, *9*, 8697–8709.
[29] O. Voznyy, J. J. Dubowski, J. T. Yates, P. Maksymovych, *J. Am. Chem. Soc.* **2009**, *131*, 12989–12993.
[30] F. L. Maza, P. Carro, C. Vericat, K. Kern, R. C. Salvarezza, D. Grumelli, *J. Phys. Chem. C* **2018**, *122*, 2207–2214.
[31] O. Stetsovych, M. Švec, J. Vacek, J. V. Chocholoušová, A. Janík, J. Rybáek, K. Kosmider, I. G. Stará, P. Jelínek, I. Starý, *Nat. Chem.* **2017**, *9*, 213–218.
[32] A. Shiotari, T. Nakae, K. Iwata, S. Mori, T. Okujima, H. Uno, H. Sakaguchi, Y. Sugimoto, *Nat. Commun.* **2017**, *8*, 16089.
[33] A. Shiotari, K. Tanaka, T. Nakae, S. Mori, T. Okujima, H. Uno, H. Sakaguchi, Y. Sugimoto, *J. Phys. Chem. C* **2018**, *122*, 4997–5003.
[34] H. Zhang, H. Liu, C. Shen, F. Gan, X. Su, H. Qiu, B. Yang, P. Yu, *Int. J. Mol. Sci.* **2019**, *20*, 2018.
[35] A. Mairena, J. I. Mendieta, O. Stetsovych, A. Terfort, I. G. Stará, I. Starý, P. Jelínek, K. H. Ernst, *Chem. Commun.* **2019**, *55*, 10595–10598.
[36] I. C. Y. Hou, Q. Sun, K. Eimre, M. di Giovannantonio, J. I. Urgel, P. Ruffieux, A. Narita, R. Fasel, K. Müllen, *J. Am. Chem. Soc.* **2020**, *142*, 10291–10296.
[37] N. Ogawa, Y. Yamaoka, H. Takikawa, K. I. Yamada, K. Takasu, *J. Am. Chem. Soc.* **2020**, *142*, 13322–13327.
[38] T. G. Lohr, J. I. Urgel, K. Eimre, J. Liu, M. di Giovannantonio, S. Mishra, R. Berger, P. Ruffieux, C. A. Pignedoli, R. Fasel, X. Feng, *J. Am. Chem. Soc.* **2020**, *142*, 13565–13572.
[39] Q. Fan, D. Martin-Jimenez, D. Ebeling, C. K. Krug, L. Brechmann, C. Kohlmeyer, G. Hilt, W. Hieringer, A. Schirmeisen, J. M. Gottfried, *J. Am. Chem. Soc.* **2019**, *141*, 17713–17720.
[40] C. Wäckerlin, A. Gallardo, A. Mairena, M. Baljozović, A. Cahlík, A. Antalík, J. Brabec, L. Veis, D. Nachtigallová, P. Jelínek, K.-H. Ernst, *ACS Nano* **2020**, *14*, 16735–16742.
[41] F. Eisenhut, T. Lehmann, A. Viertel, D. Skidin, J. Krüger, S. Nikipar, D. A. Ryndyk, C. Joachim, S. Hecht, F. Moresco, G. Cuniberti, *ACS Nano* **2017**, *11*, 12419–12425.
[42] B. Mallada, B. de la Torre, J. I. Mendieta-Moreno, D. Nachtigallová, A. Matěj, M. Matoušek, P. Mutombo, J. Brabec, L. Veis, T. Cadart, M. Kotora, P. Jelínek, *J. Am. Chem. Soc.* **2021**, *143*, 14694–14702.
[43] A. J. Stone, D. J. Wales, *Chem. Phys. Lett.* **1986**, *128*, 501–503.
[44] E. Brayfindley, E. E. Irace, C. Castro, W. L. Karney, *J. Org. Chem.* **2015**, *80*, 3825–3831.
[45] A. V. Smolobochkin, A. S. Gazizov, A. S. Melyashova, J. K. Voronina, A. G. Strelnik, S. Z. Vatsadze, A. R. Burilov, M. A. Pudovik, O. A. Fedorova, O. G. Sinyashin, *RSC Adv.* **2017**, *7*, 50955–50960.
[46] S. Luo, A. J. Kuhn, I. Castano, C. Castro, W. L. Karney, *J. Org. Chem.* **2018**, *83*, 314–322.
[47] S. M. Bachrach, *J. Phys. Chem. A* **2008**, *112*, 7750–7754.
[48] H. J. Bernstein, *Trans. Faraday Soc.* **1962**, *58*, 2285.
[49] C. Wentrup, H.-W. Winter, D. Kvaskoff, *J. Phys. Chem. A* **2015**, *119*, 6370–6376.
[50] J. I. Mendieta-Moreno, R. C. Walker, J. P. Lewis, P. Gómez-Puertas, J. Mendieta, J. Ortega, *J. Chem. Theory Comput.* **2014**, *10*, 2185–2193.
[51] X. Liu, A. Matej, T. Kratky, J. I. Mendieta-Moreno, S. Günther, P. Mutombo, S. Decurtins, U. Aschauer, J. Repp, P. Jelinek, S. Liu, L. L. Patera, *Angew. Chem. Int. Ed.* **2022**, *61*, 0; *Angew. Chem.* **2022**, *134*, 0.
[52] H. E. Winberg, F. S. Fawcet, *Org. Synth.* **1962**, *42*, 83.
[53] W. S. Trahanovsky, S. P. Lorimor, *J. Org. Chem.* **2006**, *71*, 1784–1794.
[54] X. Fu, D. Zhao, *Org. Lett.* **2015**, *17*, 5694–5697.
[55] T. Stuyver, B. Chen, T. Zeng, P. Geerlings, F. de Proft, R. Hoffmann, *Chem. Rev.* **2019**, *119*, 11291–11351.

Manuscript received: May 31, 2022
Accepted manuscript online: October 14, 2022
Version of record online: November 15, 2022